 CMES, vol.18, no.3, pp.223-234, 2007

Numerical Generation of Freak Waves Using MLPG_R and QALE-FEM Methods

Q.W. Ma[1]

Abstract: Two methods have been recently developed by the author and his group: one called MLPG_R (Meshless Local Petrov-Galerkin method based on Rankine source solution) and the other called QALE-FEM (Quasi Arbitrary Lagrangian-Eulerian Finite Element Method). The former is a meshless method developed from a general MLPG (Meshless Local Petrov-Galerkin) method and is more computationally efficient than the general one when applied to modelling nonlinear water waves. The later is a mesh-based method similar to a conventional finite element method (FEM) when discretizing the governing equations but different from the conventional one in managing the mesh. In this paper, they are applied to simulate freak waves, which has yet been done before. Comparison is made between results from these two methods and between their results and those from experiments available in literature. Good agreement is achieved.

Keyword: Freak waves; MLPG_R; QALE-FEM; nonlinear water waves.

1 Introduction

Freak waves (also called rogue waves) are extraordinarily large water waves in ocean. A literature survey has revealed that freak waves may occur in many places (shallow and deep water). Although their occurrence is considered as rare, they potentially pose severe hazards for mariners and man-made structures. Many incidents considered to be caused by freak waves have been reported, in which a lot of lives (about 542 during 1969-1994) were lost as given by Lawton (2001). It has now been recognized that freak waves are real threat to all human activities in ocean.

The freak wave phenomenon has attracted great attention. A sufficient summary can be found in a recent review by Kharif and Pelinovsky (2003). The main conclusions from this review are (i) that the physical mechanisms of freak wave generation include spatio-temporal (dispersive) focusing of transient wave groups with different wavelengths, wave-current interaction, geometrical focusing due to topography of the seabed and modulation instability; and (ii) that mathematical models based on different physical mechanisms have been suggested with various levels of approximation, which consist of linear, weakly nonlinear and fully nonlinear models, such as the energy balance equation, the wave-action balance equation, the nonlinear Schrödinger equation, the nonlinear KdV equation and the fully nonlinear model based on a potential theory.

A lot of efforts have been made to generate freak wakes in laboratory wave tanks by using wavemakers in order to gain the understanding of freak wave properties under controlled conditions. There are various methods to specify the motion of a wavemaker. Touboul, Giovanangeli, Kharif and Pelinovsky (2006) suggest that the motion of wavemaker is specified by using a sine function with linearly variable frequency with the largest frequency occurring at start. In fact, the wave train generated in this way consists of shorter waves in the front and longer waves at the tail. The shorter waves travel slower and the longer waves travel faster. At an expected time, the energy of all waves is focused at one point and so the freak wave is created. This method is similar to one proposed by Grigoropoulos, Florios and

[1] School of Engineering and Mathematical Sciences, City University, Northampton Square, London EC1V 0HB, UK. E-Mail: q.ma@city.ac.uk. Personal home page: http://www.staff.city.ac.uk/q.ma/

Loukakis (1994) for generating a transient wave, in which the wavemaker is excited by a succession of unchanged-period sine wave signals (i.e. frequency unchanged in whole period but different in different periods). The other way to specify the motion of the wavemaker is based on the sum of a number of sine (or cosine) wave components, each having a different frequency. The freak wave is formed in the wave tank when all the wave components have such a phase that their peaks take place at the same point and at the same time. Many researchers, such as Graw & Koola (1997) and Baldock, Swan & Taylor (1996), have adopted this method. Both these methods generate a large transient freak wave in water that is almost quiescent a long time before and after the freak wave occurs, which is different from reality where freak waves always appear in other random waves. In order to overcome this problem, Kriebel (2000) proposes a combined method, i.e., signals exciting the wavemaker are composed of two parts (1) for generating the normal random waves and (2) for generating the freak waves. More realistic way has been used by Clauss and his group (Clauss, 2002), in which the signal for the motion of the wavemaker is obtained by performing Fourier analysis on the real time record of sea states containing freak waves.

Numerical modelling can be performed in the similar way to the physical experiments using numerical wave tank. Nevertheless, different numerical methods and procedures may be employed. Only some of relevant publications are cited here. More references may be found in the cited papers. Touboul, Giovanangeli, Kharif and Pelinovsky (2006) use a boundary integral equation method (BIEM) and a mixed Euler Lagrange (MEL) time marching scheme. Brandini & Grilli (2001) perform the simulation of freak waves based on higher-order boundary element method. Grue, J. (2002) describe a method of successive approximations to the solution of the Laplace equation governing the fluid flow. All these methods have given very impressive numerical results.

In this paper, two newly developed methods by the author will be employed to simulate freak wave: one called MLPG_R method and the other called QALE-FEM. The former is a meshless method developed from a general MLPG method proposed by Prof. Atluri and his research group (e.g., Atluri & Zhu 1998; Lin & Atluri, 2001 and Atluri and Shen, 2002; Han, Rajendran & Atluri, 2005; Atluri, Liu & Han, 2006) and is more computationally efficient than the general one when applied to modelling nonlinear water waves. The later is a mesh-based method similar to a finite element method (FEM) when discretizing the governing equations but different from the conventional FEM in managing the mesh. The successes of the conventional FEM rely on a good mesh. The mesh may be generated with high quality but may become over-distorted during simulation since the fluid domain is continuously changing with oscillation of the free surface. To overcome the over-distortion, they must be regenerated frequently or even every time step but remeshing may take a major proportion of computational costs if an unstructured mesh are used. In the QALE-FEM, the complex mesh is generated only once at the beginning and is moved at all other time steps in order to conform to motions of the free surface and structures by using a spring analogy method specially developed for nonlinear waters waves and their interaction with fixed and floating bodies. Extensive numerical instigations have shown that the QALE-FEM can be more than 6 times faster than the conventional one. The potential of these two methods is explored in this paper by applying them to simulate freak waves, which have yet done before.

2 Generation of Freak Waves

The numerical wave tank is as shown in Fig.1. The piston-like wavemaker is mounted at the left end and a damping zone with a Sommerfeld condition (see Ma, Wu, & Eatock Taylor (2001) for details) is applied at the right end of the tank in order to suppress the reflection. A Cartesian coordinate system is used with the *oxy* (y-axis pointing toward the paper) plane on the mean free surface and with the z-axis being positive upwards. Unless mentioned otherwise, its origin is located at the mean position of the wavemaker. This is similar to the physical wave tank in laboratory.

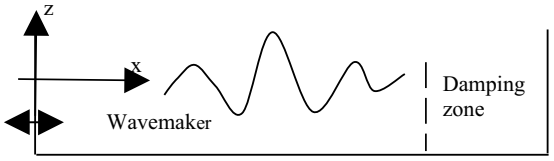

Figure 1: Sketch of numerical wave tank

The method to generate freak waves is similar to one of methods in physical experiments discussed above, i.e., by using a sum of a number of sine (cosine) wave components. The displacement of the wavemaker (e.g., Baldock, Swan & Taylor, 1996) is given by:

$$S(t) = \sum_{n=1}^{N} \frac{a_n}{F_n} \cos(\omega_n t + \varepsilon_n). \tag{1a}$$

The corresponding velocity is

$$\frac{dS(t)}{dt} = -\sum_{n=1}^{N} \frac{a_n}{F_n} \omega_n \sin(\omega_n t + \varepsilon_n). \tag{1b}$$

In the above equations, N is the total number of components. ε_n is the phase of the n-th component. k_n and ω_n are the wave number and frequency of the n-th component, respectively, and are related by $\omega_n^2 = g k_n \tanh(k_n d)$, where d is the mean water depth. The frequencies of the wave components are equally spaced over the band $[\omega_1, \omega_N]$ with ω_1 being the smallest and ω_N being the largest frequencies, respectively. a_n is the amplitude of n-th component, which is taken as the same for all components in this paper to simplify the relationship between the target amplitude (A) of the freak wave and the amplitudes of the components, leading to $a_n = a = A/N$ or $Na_n = Na = A$. F_n is the theoretical transfer function of the wavemaker given by (Dean and Dalrymple, 1991):

$$F_n = \frac{2[\cosh(2k_n d) - 1]}{\sinh(2k_n d) + 2k_n d} \tag{2}$$

As indicated by Dean and Dalrymple (1991), each component of the waves generated by using Eqs. (1)-(2) consists of two parts: one is the progressive wave and the other is the standing or local wave. The local wave decays with the increase in the distance from the wavemaker and becomes negligible after a point that is 3 or more water depths away from the wavemaker. The progressive wave consists of a transient wave profile in the front part of a harmonic wave train even though the motion of the wavemaker is purely harmonic. Therefore, the wave at a certain point downstream of the wavemaker become harmonic only after the transient wave has passed this point. Based on a linear theory (e.g., Baldock, Swan & Taylor, 1996) and choosing $\varepsilon_n = k_n x_f - \omega_n t_f$ with x_f and t_f being the focusing point and the focusing time, the wave in the tank generated by using Eqs. (1)-(2) may be expressed as

$$\zeta(x,t) = \sum_{n=1}^{N} a_n \cos[k_n(x - x_f) - \omega_n(t - t_f)] \qquad (x, x_f > x_l \text{ and } t, t_f > t_l) \tag{3}$$

where x_l represents the nearest point to the wavemaker, where the local wave is negligible and should be larger than 3 or 4 water depth; and t_l represents the time when the transient wave fronts corresponding to all the components just pass points x and x_f. Eq. (3) shows that all the wave components reach their peaks at the focusing point (x_f) and the focusing time (t_f) and so the freak wave occurs with amplitude equal to $\sum_{n=1}^{N} a_n$. It should be noted that this is true for the linear wave. When the nonlinearity is considered, the amplitude of the freak wave as well as the focusing time and position may not be the same as the ones from the linear theory.

3 Outline of numerical methods

The two methods to be used for simulating the freak waves are similar to those described in previous publications. For completeness, a brief about each of these methods will be given here. For details, readers are referred to Ma (2005) and Ma & Yan (2006).

3.1 MLPG_R method

The MLPG_R method is based on general Euler equations for fluids, which is governed by the following equations and conditions:

$$\nabla \cdot \vec{u} = 0 \qquad \text{in fluid domain} \tag{4a}$$

$$\frac{D\vec{u}}{Dt} = -\frac{1}{\rho}\nabla p + \vec{g} \quad \text{in fluid domain} \quad (4b)$$

$$\frac{D\vec{x}}{Dt} = \vec{u} \text{ and } p = p_{atm} \quad \text{on the free surface} \quad (5a)$$

$$\vec{u}.\vec{n} = \vec{U}.\vec{n} \quad \text{on rigid boundaries} \quad (5b)$$

and

$$\vec{n}.\nabla p = \rho\left(\vec{n}\cdot\vec{g} - \vec{n}\cdot\dot{\vec{U}}\right) \quad \text{on rigid boundaries} \quad (5c)$$

where, ρ is the density of fluids, $\vec{u}$ the velocity of fluids, $\vec{U}$ the velocity of rigid boundaries, $\vec{g}$ the gravitational acceleration, p the pressure and p_{atm} the atmospheric pressure that can be taken as zero without loss of generality.

The problem defined by above equations is solved using a time-step marching procedure. In this procedure, intermediate velocities and positions are first estimated by

$$\vec{u}^{(*)} = \vec{u}^{(n)} + \vec{g}\Delta t \quad (6)$$

$$\vec{r}^{(*)} = \vec{r}^{(n)} + \vec{u}^{(*)}\Delta t \quad (7)$$

where $\vec{r}$ is the position vector of a point; Δt is the time step; and the superscripts (n) indicate the quantities at time $t = t_n$. The velocities at time $t = t_{n+1} = t_n + \Delta t$ is then expressed by

$$\vec{u}^{(n+1)} = \vec{u}^{(*)} + \vec{u}^{(**)}. \quad (8)$$

Integrating Eq. (4b) over the time interval (t_n, t_{n+1}) results in

$$\vec{u}^{(n+1)} = \vec{u}^{(n)} + \vec{g}\Delta t - \int_{t_n}^{t_{n+1}} \left(\frac{1}{\rho}\nabla p\right) dt. \quad (9)$$

With use of the well-known approximation to the time integration, we have

$$\int_{t_n}^{t_{n+1}} \left(\frac{1}{\rho}\nabla p\right) dt = \Delta t\left[\frac{\theta}{\rho}\nabla p^{(n+1)} + \frac{1-\theta}{\rho}\nabla p^{(n)}\right] \quad (10)$$

The velocity in Eq. (9) becomes

$$\vec{u}^{(n+1)} = \vec{u}^{(*)} - \Delta t\left[\frac{\theta}{\rho}\nabla p^{(n+1)} + \frac{1-\theta}{\rho}\nabla p^{(n)}\right] \quad (11)$$

The velocity in Eqs. (8) and (11) must also satisfy the continuity equation (4a), yielding

$$\nabla^2 p^{(n+1)} = \frac{\rho}{\theta\Delta t}\nabla\cdot\vec{u}^{(*)} - \left(\frac{1}{\theta} - 1\right)\nabla^2 p^{(n)}. \quad (12)$$

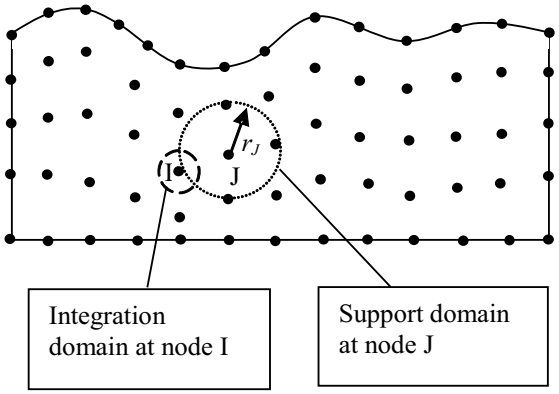

Figure 2: Illustration of nodes, integration domain and support domain

It is clear that this formulation is not suitable for θ=0, though it could be any value in the range of $0 < \theta \leq 1$. In this paper, the fully implicit method (θ=1) is employed, leading to

$$\vec{u}^{(n+1)} = \vec{u}^{(*)} - \frac{\Delta t}{\rho}\nabla p^{(n+1)} \quad (13)$$

and

$$\nabla^2 p^{(n+1)} = \frac{\rho}{\Delta t}\nabla\cdot\vec{u}^{(*)}. \quad (14)$$

Eq. (14) governs the pressure at the new time level, from which the solution for it can be found. After finding the solution for $p^{(n+1)}$, one may estimate the velocities by using Eq. (13). The positions of fluid particles can then be updated by numerically integrating the velocities.

In order to solve Eq. (14), the MLPG_R method may be employed. This method is based on a set of nodes (Fig. 2), which discretise the fluid domain, as in the general MLPG (e.g., Atluri, Han & Shen, 2003; Sladek, Sladek, Atluri, 2001; Sladek, Sladek, Zhang, Garcia-Sanche, Munsche 2006; Han, Rajendran & Atluri, 2005; Atluri, Liu &

Han, 2006). The weak form for this method on each integration domain can be expressed as follows:

$$\int_{\partial\Omega_I} \vec{n}\cdot(p\nabla\varphi)\,dS - p = \int_{\Omega_I} \frac{\rho}{\Delta t}\vec{u}^{(*)}\cdot\nabla\varphi\,d\Omega \qquad (15)$$

where ϕ is the test function, satisfying that $\nabla^2\varphi = 0$, in Ω_I except for its centre and $\varphi = 0$, on $\partial\Omega_I$, the boundary of Ω_I, which may be given by:

$$\varphi = \frac{1}{4\pi}\begin{cases} 2\ln(r/R_I) & \text{for a two dimensional case} \\ (1-R_I/r) & \text{for a three dimensional case} \end{cases} \qquad (16)$$

where r is the distance between a concerned point and the centre of Ω_I; and R_I is the radius of Ω_I.

The domain integral on the right hand side of Eq. (15) may be further expressed as

$$\int_{\Omega_I} \frac{\rho}{\Delta t}\vec{u}^{(*)}\cdot\nabla\varphi\,d\Omega = \frac{\rho}{2\pi\Delta t}\int_0^{2\pi}\int_0^{R_I} u_r^{(*)}(r,\theta)\,dr d\theta \qquad (17)$$

for 2D cases (similarly for 3D cases but not given here, see Ma, 2005), where $u_r^{(*)}$ is the radial component of $\vec{u}^{(*)}$. The integral may be numerically evaluated by using the Gaussian quadrature. To do so, more than 16 Gaussian points for 2D case (and 64 Gaussian points for 3D cases) may be required to obtain satisfactory results for the intermediate velocities. Evaluation of them at so many points is time-consuming. In order to make the method more efficient, a semi-analytical technique is developed which is based on the following methodology:

1) Dividing an integration domain into several sub-domains (Fig. 3);

2) Assuming intermediate velocities to linearly vary over each subdomain;

3) Performing the integration over each subdomain analytically.

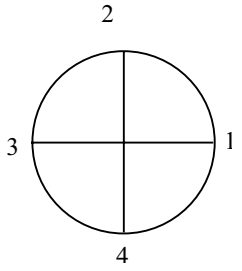

Figure 3: Illustration of division of an integration domain.

Using this methodology, the integral in Eq. (17) for 2D cases is expressed by

$$\begin{aligned}&\int_0^{2\pi}\int_0^{R_I} u_r^{(*)}(r,\theta)\,dr d\theta \\ &= \sum_{i=1}^{N_I}\frac{R_I}{4}\Big[(c_{uxi}+c_{wzi})(\vartheta_{i+1}-\vartheta_i) \\ &+ (c_{uxi}-c_{wzi})(\sin\vartheta_{i+1}\cos\vartheta_{i+1}-\sin\vartheta_i\cos\vartheta_i) \\ &\quad + (c_{uzi}+c_{wxi})\left(\sin^2\vartheta_{i+1}-\sin^2\vartheta_i\right)\Big] \end{aligned} \qquad (18)$$

where ϑ_i (i=1,2,...) is the polar angle of a dividing point (such as 1 or 2 in Fig. 3); and the coefficients c_{uxi} and c_{uyi} are evaluated, respectively, by

$$c_{uxi} = \frac{\left(u_i^{(*)}-u_0^{(*)}\right)(z_{i+1}-z_0)-\left(u_{i+1}^{(*)}-u_0^{(*)}\right)(z_i-z_0)}{(x_i-x_0)(z_{i+1}-z_0)-(x_{i+1}-x_0)(z_i-z_0)}R_I \qquad (19a)$$

$$c_{uyi} = \frac{(x_i-x_0)\left(u_{i+1}^{(*)}-u_0^{(*)}\right)-(x_{i+1}-x_0)\left(u_i^{(*)}-u_0^{(*)}\right)}{(x_i-x_0)(z_{i+1}-z_0)-(x_{i+1}-x_0)(z_i-z_0)}R_I \qquad (19b)$$

where $u_0^{(*)}$ and $u_i^{(*)}$ are the velocity components in x- directions at the center of the subdomain and the dividing point (i) respectively. The coefficients c_{wxi} and c_{wzi} can be found similarly or obtained by replacing $\left(u_i^{(*)}, u_{i+1}^{(*)}\right)$ with $\left(w_i^{(*)}, w_{i+1}^{(*)}\right)$, the velocity components in z-direction.

It should be noted that with this semi-analytical technique, the velocities at only five points for a 2D case with four divisions, instead of at more than 16 points if the Gaussian quadrature would be used, need to be evaluated. In 3D cases, the

spherical domain may be divided in to 8 subdomains as indicated above and the velocities at only 7 points need to be evaluated, instead of at least 64 points when using the Gaussian quadrature. As a result, the reduction in CPU time spent on the evaluation of the domain integral is considerable. This technique was employed to simulate various water waves, such as the propagating steep wave and the sloshing wave in Ma (2005). Numerical tests showed that dividing each integration domain into four subdomains can achieve the relative accuracy of less than 1% (in term of mean error) for 2D cases.

3.2 QALE-FEM method

The QALE-FEM method is based on a fully nonlinear potential theory (FNPT) for water waves. In this model the velocity is computed from a velocity potential (ϕ) that satisfies the following governing equations and boundary conditions:

$$\nabla^2\phi = 0 \qquad \text{in fluid domain} \quad (20)$$

$$\frac{Dx}{dt} = \frac{\partial\phi}{\partial x} \quad \text{on the free surface } z = \zeta(x,y,t) \quad (21a)$$

$$\frac{Dy}{dt} = \frac{\partial\phi}{\partial y} \quad \text{on the free surface } z = \zeta(x,y,t) \quad (21b)$$

$$\frac{Dz}{dt} = \frac{\partial\phi}{\partial z} \quad \text{on the free surface } z = \zeta(x,y,t) \quad (21c)$$

$$\frac{D\phi}{Dt} = -gz + \frac{1}{2}|\nabla\phi|^2 \quad \text{on the free surface } z = \zeta(x,y,t) \quad (22)$$

$$\frac{\partial\phi}{\partial n} = \vec{n}\cdot\vec{U}(t) \qquad \text{on rigid boundary} \quad (23)$$

where $\vec{U}(t)$ and $\vec{n}$ is the velocity and the unit normal vector of the rigid boundaries, respectively.

As has been known, the FEM may require less memory and, therefore, may be computationally more efficient than the BEM for solving fully nonlinear wave problems, as indicated by Ma, Wu & Eatock Taylor (2001). The disadvantage of the FEM, however, is that a complex unstructured mesh is generally required and may need to be remeshed at every time step to follow the motion of waves and/or structures. To overcome the difficulty, the QALE-FEM has been recently invented (Ma & Yan, 2006) to solve Eqs. (20) to (23). In this method the complex mesh is generated only once at the beginning and is moved at all other time steps in order to conform to the motion of the free surface and/or structures. Based on numerical tests so far, the QALE-FEM requires less than 15% of the CPU time required by the conventional FEM at the same accuracy level.

There are three key elements in this method, including the mesh moving, velocity calculation and implicit iteration procedure to solve fully coupled problems about the interaction between water waves and floating structures. The third element is not concerned here because the floating structures are not considered in this paper. Details about it can be found in Yan & Ma (2006). Other two elements are outlined as follows.

The novel methodology for moving mesh is that interior nodes and boundary nodes are considered separately; the nodes on the free surface and on rigid boundaries are considered separately; nodes on the free surface are split into two groups: those on waterlines and those not on waterlines (inner-free-surface nodes); and different methods are employed for moving different nodes. To move the interior nodes which do not lie on boundaries, a spring analogy method is used. In this method, nodes are considered to be connected by springs and the whole mesh is then deformed like a spring system. Specifically, the nodal displacement is determined by

$$\Delta\vec{r}_i = \sum_{j=1}^{N_i} k_{ij}\Delta\vec{r}_j \Big/ \sum_{j=1}^{N_i} k_{ij} \qquad (24)$$

where $\Delta\vec{r}_i$ is the displacement at Node I; k_{ij} is the spring stiffness and N_i is the number of nodes that are connected to Node I. For problems about nonlinear water waves, it is crucial to maintain the quality (good element shapes and reasonable node distribution) of mesh near the free surface. To do so, the spring stiffness in the QALE-FEM for the case without floating structures is suggested as

$$k_{ij} = \frac{1}{l_{ij}^2} e^{\gamma\left[1+\left(z_i+z_j\right)/2d\right]} \qquad (25)$$

where k_{ij} is the spring stiffness, l_{ij} is the distance between Nodes I and J; z_i and z_j are the vertical coordinates of Nodes I and J; $d$is the water depth; and γ is an coefficient that should be assigned a larger value if the springs are required to be stiffer at the free surface. The term $1+(z_i+z_j)/2d$ represents the distance between the element concerned and the surface, measured in its normal direction in calm water, which may be updated but it is not necessary to do so unless the overturning wave are considered. The spring analogy method is also used for moving nodes on rigid boundaries.

The positions of nodes on the free surface are determined by physical boundary conditions, i.e., following the fluid particles at most time steps. The nodes moved in this way may become too close to or too far from each other. To prevent this from happening, these nodes are relocated at a certain frequency, e.g. every 40 time steps. When doing so, the nodes on the waterlines is re-distributed according to a principle for a self-adaptive mesh, i.e., the weighted arc-segment lengths satisfies

$$\varpi_i \Delta s_i = C_s \tag{26}$$

where ϖ is a weighted function, Δs_i the arc-segment length between two successive nodes and C_s a constant. In order to relocate the inner-free-surface nodes, they are first moved using the spring analogy system in the projected plane of the free surface, resulting in new coordinates in the horizontal plane; and then the elevations of the free surface corresponding to the new coordinates are evaluated by an interpolating method. In order to take into account of the local gradient of the free surface, however, the spring stiffness for moving the nodes in x- and y- directions is determined, respectively, by:

$$k_{ij}^{(x)} = \frac{1}{l_{ij}^2}\sqrt{1+\left(\frac{\partial \zeta}{\partial x}\right)^2} \tag{27a}$$

and

$$k_{ij}^{(y)} = \frac{1}{l_{ij}^2}\sqrt{1+\left(\frac{\partial \zeta}{\partial y}\right)^2}, \tag{27b}$$

where $k_{ij}^{(x)}$ and $k_{ij}^{(y)}$ are the spring stiffness; $\frac{\partial \zeta}{\partial x}$ and $\frac{\partial \zeta}{\partial y}$ the local slopes of the free surface in the x- and y-directions, respectively. This technique for moving free surface nodes may be replaced by one based on a local coordinate system as discussed in Yan and Ma (2006), which may deal with multi-valued surfaces such as in cases of overturning waves. The resulting mesh at each time step is arbitrarily unstructured in general and changing from one time step to another.

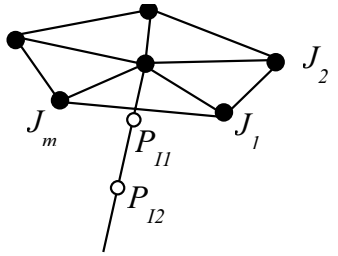

Figure 4: Nodes around Node I

In order to calculate the fluid velocity on the free surface under such a condition, an effective method is developed. In this method, the velocity at a node I with neighbours J_k ($k = 1,2,3,\ldots\ldots,m$) on the free surface is split into normal and tangential components (see Fig. 4). To estimate the normal component of the velocity, two points on the normal line at Node I are selected firstly and the velocity potentials at these two points are then approximated by using a moving least square method. The normal component ($\vec{u}_n$) of the velocity is determined by a three-point finite difference scheme:

$$\vec{u}_n = \left[\frac{2}{3h_{I1}}\left(\frac{2h_{I1}+h_{I2}}{h_{I1}+h_{I2}}+\frac{1}{2}\right)\phi_I - \left(\frac{2}{3h_{I2}}+\frac{1}{h_{I1}}\right)\phi_{I1}+\frac{2}{3h_{I2}}\left(\frac{h_{I1}}{h_{I1}+h_{I2}}\right)\phi_{I2}\right]\vec{n}, \tag{28}$$

where $I1$ and $I2$ represent the two points selected; h_{I1} and h_{I2} are the distances between I and $I1$ and between $I1$ and $I2$, respectively; and ϕ_I, ϕ_{I1} and ϕ_{I2} denote the velocity potentials at the node and the two points; the later two, ϕ_{I1} and ϕ_{I2}, are found by a moving least square method. After the normal component of the velocity is determined,

the tangential components of the velocity is calculated using a least square method based on the following equation

$$\vec{u}_{\tau_x} \cdot \vec{l}_{IJ_k} + \vec{u}_{\tau_y} \cdot \vec{l}_{IJ_k} = \vec{l}_{IJ_k} \cdot \nabla\phi - \vec{u}_n \cdot \vec{l}_{IJ_k} \quad (k = 1,2,3,\ldots\ldots,m) \quad (29)$$

where $\vec{l}_{IJ_k}$ is the unit vector from Node I to Node J_k; $\vec{u}_{\tau_x}$ and $\vec{u}_{\tau_y}$ represent the velocity components in $\vec{\tau}_x$ and $\vec{\tau}_y$ directions, respectively. These directions are determined by $\vec{\tau}_x \perp \vec{n}$, $\vec{\tau}_x // \vec{e}_x$, $\vec{\tau}_y \perp \vec{n}$ and $\vec{\tau}_y // \vec{e}_y$, where $\vec{e}_x$ and $\vec{e}_y$ are the unit vectors in the x- and y-directions, respectively.

4 Numerical examples

Numerical results for two cases will be presented in this section. In the following presentation, all parameters with a length scale are nondimensionalised by the water depth d; the time and frequency are nondimensionalised as $t \to t\sqrt{d/g}$ and $\omega \to \omega\sqrt{g/d}$.

In the first case, comparison with experimental results is made to valid these numerical methods described above for the applications to freak waves. For this purpose, the exact same motion of the wavemaker as in Nestegard (1999) is used, whose time history is plotted in Fig.5. A scaling factor may multiply the time history to obtain different amplitude of waves. Two factors (0.612 and 0.749, respectively) are considered here. In order to simulate this case, the tank length is chosen as 20. Fig. 6 shows the wave time histories recorded at $x = 13.436$ (where the largest wave amplitude is expected to occur) computed by two methods together with the experimental data given in Nestegard (1999) for the scaling factors equal to 0.612 and 0.749. In these figures, the relative error of both numerical results to those from experiments at the peak is less than 8%. The agreement of the numerical results from the two methods with the experimental data is satisfactory.

The second case is to model the freak waves generated by using Eqs. (1) - (2). In order to do so, the parameters N, Na , ω_n, x_f and must be selected. The minimum and maximum frequencies represent the band width and the centre of the wave spectrum of the targeted freak waves. In

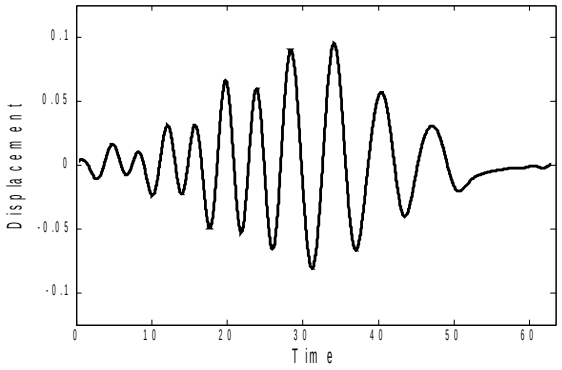

Figure 5: Time history of wavemaker motion

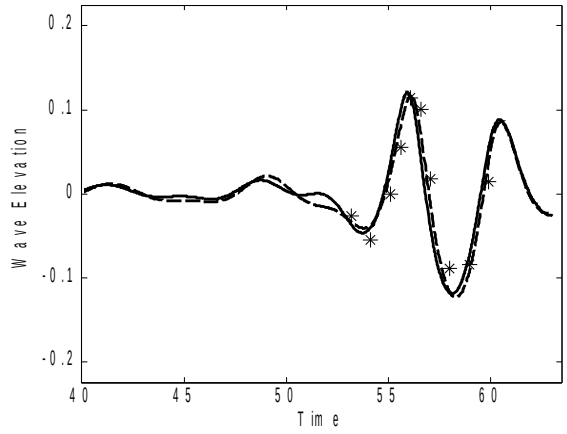

(a) Scaling factor =0.612

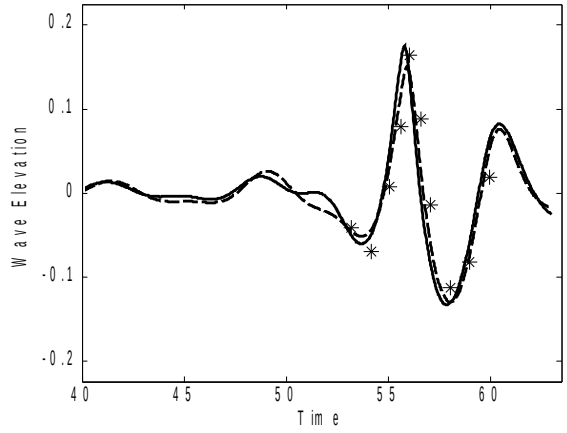

(b) Scaling factor =0.749

Figure 6: Time histories at x=13.436 with different scaling factors (Solid line: QALE-FEM; Dashed line: MLPG_R; Star: experimental data)

this work, they are selected as $\omega_1 = 0.8683$ and $\omega_n = 1.8865$. The number (N) of wave components affects the continuity of the wave spectrum and depends on the band with ($\omega_n - \omega_1$) of spectrum. If it is not large enough, the wave spectrum is not smooth and the properties of generated waves depend on the number. Based on our numerical tests, the waves are almost the same when N >20 for the above frequencies specified. It is taken as 32 in this paper. The total amplitude (Na) reflects the height of freak waves. Two values of amplitudes (Na=0.074 and 0.1488) are considered to look at the influence of different amplitudes. and t_f mainly affect the focusing point and time. According to the discussions in Section 2, must be large enough so that the local wave generated by the wavemaker should become negligible in the region where the target freak wave occurs. This requires that the nearest point of the wave pack to the wavemaker should be 3 or more water depths away from the wavemaker. t_f must also be large enough so that the shortest wave components have passed point x_f when the freak wave occurs. For the conservative reason, the nondimensional focusing point coordinate and the focusing time in Eqs. (1) - (2) are taken as x_f=14.65 and t_f=83.68 respectively. The tank length for this case is selected as 38, much longer than the distance from the wavemaker to the theoretical focusing point, and thus the focusing wave is hardly affected by the reflection even without the artificial damping zone. The wave elevations in the part of the tank (from x=5 to x=25; waves in other parts are very small and not interesting) measured from the mean free surface at two instants calculated by the two numerical methods are depicted in Fig. 7. In these two figures, the relative error between the numerical results at the peaks from both the methods is about 3%. The agreement between them in this case can be considered as good.

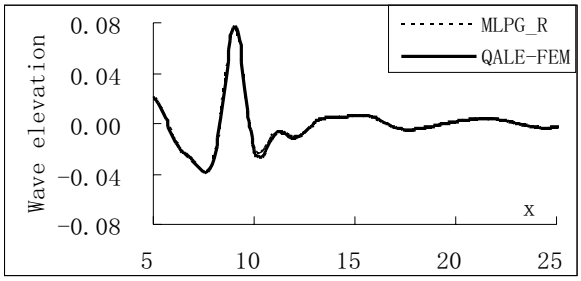

(a) t=66.0

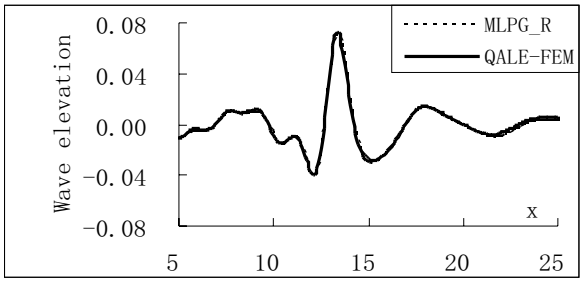

(b) t=77.25

Figure 7: Wave profiles obtained by two methods

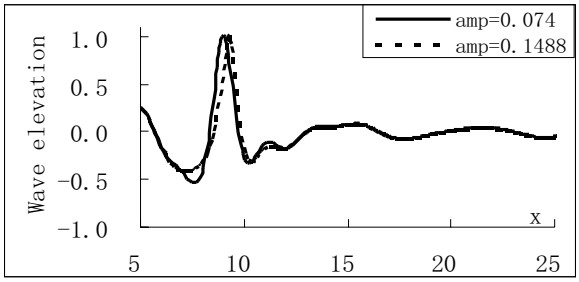

(a) t=66.0

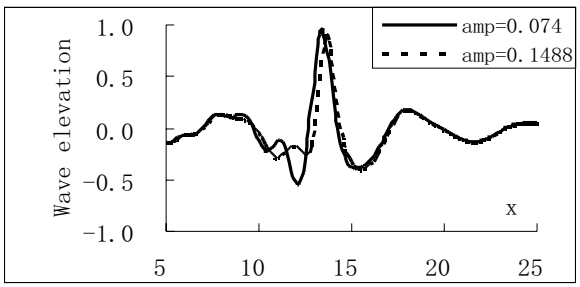

(b) t=77.25

Figure 8: Wave profiles for different amplitudes

To look at the influence of the amplitude, the results corresponding to two amplitudes obtained by the MLPG_R method are presented in Fig. 8, for which other parameters are the same as for Fig. 7. In order to show the influence of the amplitude, the wave elevations in Fig. 8 have been di-

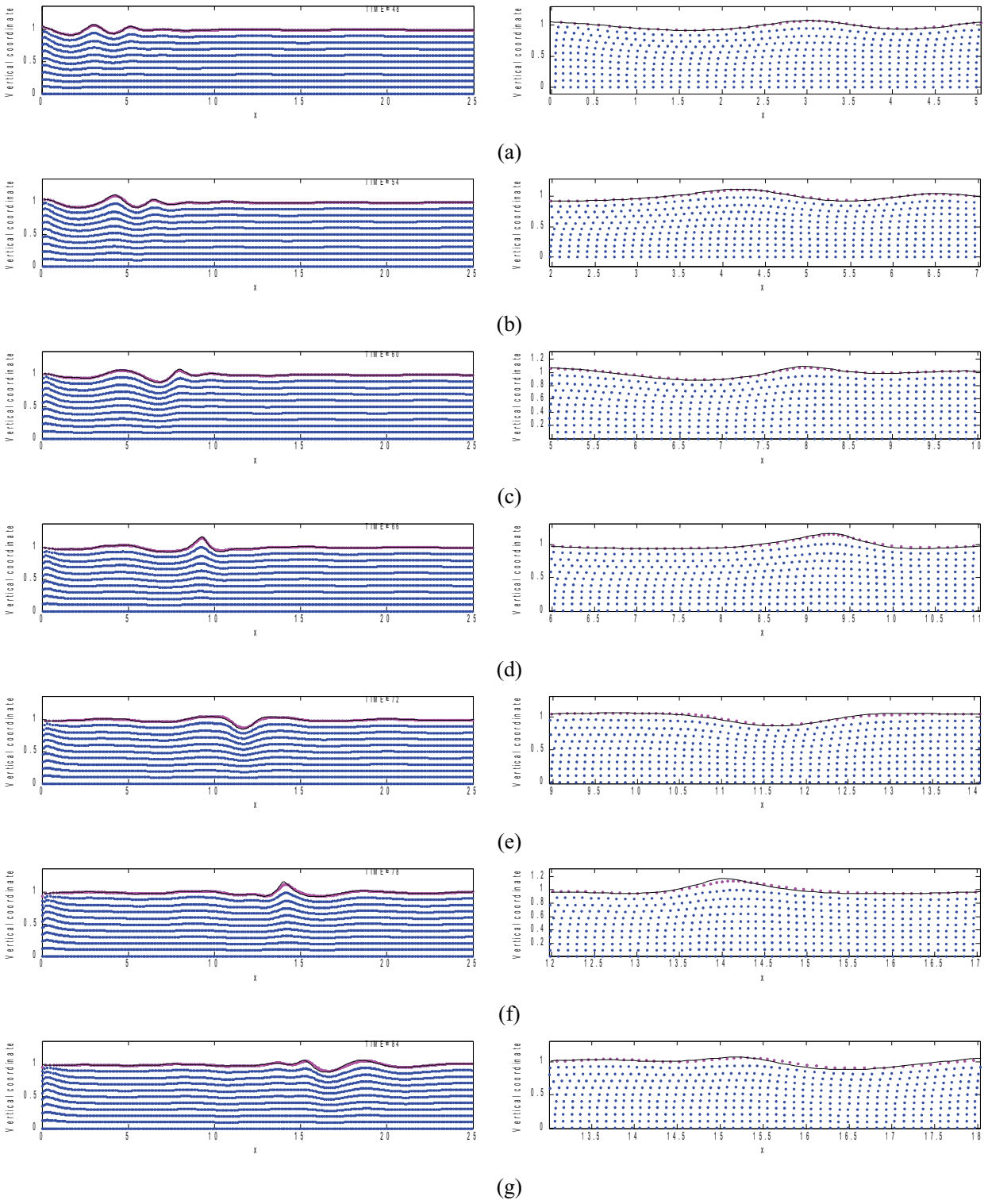

Figure 9: Node configuration from the MLPG_R method (dots) and the frees surface from the QALE-FEM (solid line) for the case with $Na = 0.1488$. The right column is the enlargement of area around the largest waves in left column.

vided by the value of Na. One may see from Fig. 8 that the wave corresponding to the larger amplitude tends to travel faster, which implies that the focusing point takes place further downstream than those to the smaller amplitude, being consistent with that observed in physical experiments (see e.g. Baldock, Swan & Taylor, 1996). The results from QALE-FEM are almost the same but not presented in Fig. 8 for clarity.

More results for the larger amplitude $Na = 0.1488$ are depicted in Fig. 9 showing that the wave packet is evolving into a large wave event at about t=78. In the figure, the dots represent the positions of nodes at the time shown on the upper-right corner of the left column obtained by the MLPG_R method. The free surface resulting from the QALE-FEM method is denoted by solid lines. The right column is the enlargement of the area around the largest wave in the left column. As can be seen, the results from the two methods are very close, though the small difference (less than about 4% at peak points) is visible in the enlarged figures. One of possible reasons for the difference may be due to the fact that the mathematical formulations in the two methods are different as described in Section 3.

5 Conclusions

This paper presents the application of the two newly-developed methods, MLPG_R and QALE-FEM, to the simulation of the freak waves. The freak waves are generated by using a piston wave-maker based on the energy focusing mechanism. The studies on two cases show that both methods can effectively model the freak waves and can give similar results and also that their results are in satisfactory agreement with experimental data as indicated by comparison with a set of published experimental data in one case.

Acknowledgement: This work is sponsored by The Leverhulme Trust (F/00 353/E), UK, for which the authors are most grateful.

References

Atluri, S.N.; Zhu, T (1998): A New Meshless Local Petrov-Galerkin (MLPG) Approach in Computational Mechanics, *Computational Mechanics,* Vol. 22, pp. 117-127.

Atluri ,S.N.; Shen ,S. (2002): The Meshless Local Petrov-Galerkin (MLPG) Method: A Simple & Less-costly Alternative to the Finite Element and Boundary Element Methods, *CMES: Computer Modelling in Engineering & Sciences*, Vol. 3 (1), pp. 11-52.

Atluri, SN; Han, ZD; Shen, S. (2003): Meshless local Petrov-Galerkin (MLPG) approaches for solving the weakly-singular traction & displacement boundary integral equations, *CMES: Computer Modeling in Engineering & Sciences*, Vol.4, No. 5, pp. 507-517.

Atluri, S. N.; Liu, H. T.; and Han, Z. D. (2006): Meshless Local Petrov-Galerkin (MLPG) Mixed Finite Difference Method for Solid Mechanics, *CMES: Computer Modeling in Engineering & Sciences*, Vol. 15, No. 1, pp. 1-16.

Baldock, T.E.; Swan, C; Taylor, P.H. (1996): A laboratory study of non-linear surface waves on water. *Philos. Trans. R. Sot. London, Ser. A*, Vol. 354, pp.l-28.

Brandini, Carlo; Grilli, St'ephan (2001): Modeling of freak wave generation in a 3D-NWT, *In. Proc. 11th Offshore and Polar Engng. Conf. (ISOPE01)*, Stavanger, Norway.

Clauss, Gunther F. (2002): Task-related rogue waves embedded in extreme seas
Proceedings of the International Conference on Offshore Mechanics and Arctic Engineering - OMAE, Vol. 4, pp. 653-665.

Dean, R. G.; Dalrymple, R.A. (1991): Water Wave Mechanics for Engineers and Scientists, World Scientific Publishing Co., ISBN 981-02-0420-5.

Grigoropoulos, G. J. , Florios, N. S. and Loukakis, T. A. (1994): Transient waves for ship and floating structure testing, *Applied Ocean Research*, Vol. 16, Issue 2, pp. 71-85.

Grue, J. (2002): On four highly nonlinear phenomena in wave theory and marine hydrodynam-

ics, *Applied Ocean Research,* Vol. 24, Issue 5, pp. 261-274.

Han, Z. D.; Rajendran, A. M.; and Atluri, S.N. (2005): Meshless Local Petrov-Galerkin (MLPG) Approaches for Solving Nonlinear Problems with Large Deformations and Rotations, *CMES: Computer Modeling in Engineering & Sciences*, Vol. 10, No. 1, pp. 1-12.

Kai-Uwe Graw; Paul Mario Koola (1997): Impact Loads on Platforms above the Sea Level due to Freak Waves, *LACER (Leipzig Annual Civil Engineering Report)* No. 2, pp. 223-230.

Kharif, C.; Pelinovsky, E., (2003): Physical mechanisms of the rogue wave phenomenon. *European Journal Mechanics B / Fluid*, 22, 603-634.

Kriebel, David L. (2000): Efficient Simulation of Extreme Waves in a Random Sea, *Rogues Waves 2000*, Brest, France.

Lawton, G., (2001): Monsters of the deep (The perfect wave), *New Scientist, Vol.* 170 (2297), pp. 28–32.

Lin H.; Atluri S.N. (2001): The Meshless Local Petrov-Galerkin (MLPG) method for solving incompressible Navier-Stokes equations, *CMES: Computer Modeling in Engineering & Sciences*, Vol. 2, No. 2, pp.117-142.

Ma, Q.W., Wu, G.X., Eatock Taylor, R., (2001): Finite element simulation of fully non-linear interaction between vertical cylinders and steep waves. Part 1: Methodology and numerical procedure, *Int.J.Numer. Meth. Fluids*, Vol. 36, pp. 265-285.

Ma, Q.W., (2005): MLPG Method Based on Rankine Source Solution for Simulating Nonlinear Water Waves, *CMES: Computer Modeling in Engineering & Sciences,* Vol. 9, No. 2, pp. 193-210.

Ma, Q.W. and Yan, S., (2006): Quasi ALE finite element method for nonlinear water waves, *Journal of Computational Physics,* Vol. 212, Issue 1, pp. 52-72.

Nestegard, A. (1999): Status of Nonlinear hydrodynamic modelling, *Technical report*, DNV, Norway.

Sladek, J.; Sladek, V.; Atluri, S.N. (2001): A Pure Contour Formulation for the Meshless Local Boundary Integral Equation Method in Thermoelasticity, *CMES: Computer Modeling in Engineering & Sciences,* Vol.2, No.4, pp. 423-434.

Sladek, J.; Sladek, V.; Zhang, Ch.; Garcia-Sanche, F.; Munsche, W. (2006): Meshless Local Petrov-Galerkin Method for Plane Piezoelectricity, *CMC: Computers, Materials & Continua*, Vol. 4, No. 2, pp. 109-118.

Touboul, J. Giovanangeli, J.P., Kharif, C and Pelinovsky, E. (2006): Freak waves under the action of wind: experiments and simulations, *European Journal of Mechanics - B/Fluids*, Vol. 25, Issue 5, pp. 662-676.

Yan, S. and Ma, Q.W., (2006): Numerical simulation of fully nonlinear interaction between steep waves and 2D floating bodies using QALE-FEM method", *Journal of Computational Physics*, Vol. 221, Issue 2, pp. 666-692.